Acta Cryst. (1975). B31, 1730

The Crystal Structure of Calcium Pyrophosphate Dihydrate*

BY NEIL STANLEY MANDEL†

Arthur Amos Noyes Laboratory of Chemical Physics, California Institute of Technology, Pasadena, California 91125, *U.S.A.*

(*Received* 21 *October* 1974; *accepted* 23 *January* 1975)

Crystals of calcium pyrophosphate dihydrate, $Ca_2P_2O_7.2H_2O$, are triclinic, space group $P\bar{1}$, with $a=7{\cdot}365$ (4), $b=8{\cdot}287$ (4), $c=6{\cdot}691$ (4) Å, $\alpha=102{\cdot}96$ (1)°, $\beta=72{\cdot}73$ (1)°, and $\gamma=95{\cdot}01$ (1)°. There are two formula units per unit cell. Data were collected on an automated diffractometer at 25 °C using Mo $K\alpha$ radiation; the structural parameters were refined to an R index of 0·037 for 4685 reflections. The six P–O_T (terminal) bond lengths range from 1·499 (1) to 1·538 (1) Å, with an average of 1·517 Å; the two P–O_B (bridge) lengths are equal at 1·623 (1) Å. Average angles are O_B–P–O_T, 107°, and O_T–P–O_T, 112°; the P–O_B–P angle is 123·1 (1)°. A survey of known pyrophosphate structures shows the pyrophosphate anion to be extremely flexible and capable of adopting varied conformations with different cations. The two water molecules form one inter-water hydrogen bond and three hydrogen bonds to the pyrophosphate oxygens. Both calcium atoms are seven coordinated at Ca···O distances less than 2·7 Å.

Introduction

The determination of the structure of calcium pyrophosphate dihydrate was undertaken as part of a program of research on the structures of compounds responsible for the inflammatory process in acute gouty arthritis. Calcium pyrophosphate dihydrate crystals are found *in vivo* in the inter-articular spacing in knee joints. When the gouty-type inflammation is caused by calcium pyrophosphate crystals, the syndrome is called chondrocalcinosis or pseudogout. Crystals of calcium pyrophosphate dihydrate cause the membrane of the digestive organelle, the lysosome, to rupture, allowing the lysosome's digestive enzymes to escape and begin the digestion of their parent white blood cell. This self digestion ends in the loss of viability of the polymorphonuclear leukocyte, increasing the amount of general inflammation.

Experimental

Naturally occurring *in vivo* crystals of calcium pyrophosphate dihydrate have been observed in the form of prisms elongated along their prism axis with their needle length being 1–20 μm. Synthetic crystals of the dihydrate in the form of prismatic parallelepipeds were grown by slow evaporation of calcium acid pyrophosphate ($CaH_2P_2O_7$) from water at room temperature (Brown, Lehr, Smith & Frazier, 1963). These synthetic crystals were compared with numerous *in vivo* crystalline samples from synovial effusions by powder analysis using a Guinier–Hägg camera. This camera, which is equipped with a focusing quartz crystal monochromator, was designed and constructed locally with the guidance of machine drawings supplied to Dr S. Samson by Professor G. Hägg, University of Uppsala. The major features of all patterns obtained from the *in vivo* crystals agreed well with the pattern for the synthetic material. There were, however, extra lines in some of the *in vivo* patterns which were apparently due to calcium hydroxyapatite (human bone) fragments.

Preliminary precession and Weissenberg photographs suggested a triclinic crystal system and gave approximate cell dimensions; more accurate cell constants were obtained by a least-squares fit to 2θ values measured on a diffractometer. The density was measured both by flotation (this work) and by refractive studies (Brown *et al.*, 1963). Crystal data are given in Table 1.

Table 1. *Crystal data*

$Ca_2P_2O_7.2H_2O$	λ(Mo $K\alpha$) = 0·71069 Å
Space group $P\bar{1}$	F.W. 290·14
$a=7{\cdot}365$ (4) Å	$Z=2$
$b=8{\cdot}287$ (4)	$F_{000}=292$
$c=6{\cdot}691$ (4)	$D_{calc}=2{\cdot}56$ g cm^{-3}
$\alpha=102{\cdot}96$ (1)°	$D_{flot}=2{\cdot}55$ g cm^{-3}
$\beta=72{\cdot}73$ (1)	$D_{R\ index}=2{\cdot}46$ g cm^{-3}
$\gamma=95{\cdot}01$ (1)	$\mu=18{\cdot}97$ cm^{-1}

Intensity data were measured on a Datex-automated General Electric diffractometer using Mo $K\alpha$ radiation with a graphite monochromator. The crystal had approximate dimensions 0·12 × 0·15 × 0·33 mm and was mounted along **c**, the long prism axis. Reflections with $2\theta \leq 80{\cdot}0°$ were scanned in the θ–2θ mode at a rate of 1° min^{-1}, the scan range varying linearly from 4·0° at $2\theta=4{\cdot}0°$ to 5·5° at $2\theta=80{\cdot}0°$. A 30 background count was measured on either side of the scan range.

Two equivalent sets of data were collected and averaged to yield the final 4684 unique reflections used in the structural solution.* Three check reflections were measured every 50 reflections; the intensities of these

* Contribution No. 5000 from the Arthur Amos Noyes Laboratory of Chemical Physics.

† NIH Postdoctoral Fellow.

* The structure-factor table has been deposited with the British Library Lending Division as Supplementary Publication No. SUP 30938 (22 pp., 1 microfiche). Copies may be obtained through The Executive Secretary, International Union of Crystallography, 13 White Friars, Chester CH1 1NZ, England.

reference reflections varied ±2% during the entire data collection. Corrections were not made for this fluctuation or for absorption ($\mu r_{max}=0{\cdot}4$). Each reflection was assigned a variance $\sigma^2(I)$ based on counting statistics plus an empirical term $(0{\cdot}02S)^2$ where S is the total scan count. Values of F_o^2 and $\sigma(F_o^2)$ were derived from the net intensities by application of the Lorentz and polarization factors.

Structure solution and refinement

The structure was solved by direct methods. Symbolic addition using three origin reflections and four symbols led to a set of 92 hand-calculated phases. Inter-symbol equivalences reduced the number of possible solutions to four, one of which was the trivial solution with all signs positive. E maps were calculated for the three remaining solutions. Two of these solutions led to E maps with 30 or 40 random peaks, while the third solution yielded both calcium atoms and the entire pyrophosphate anion. A subsequent electron-density map indicated the positions of the two oxygen atoms of the water molecules. Four cycles of full-matrix least-squares adjustment of the coordinates and isotropic temperature factors ended in an R $[=\sum(||F_o|-|F_c||)/\sum|F_o|]$ of 0·06. The four hydrogen atoms were then located on a difference map. Further full-matrix refinement of 135 parameters – coordinates of all 17 atoms, anisotropic temperature factors for the 13 heavy atoms, isotropic temperature factors for the four hydrogen atoms, a secondary extinction parameter (Larson, 1967), and a scale factor – led to a final R index of 0·037, a weighted R_w $[=\{\sum w(|F_o|^2-|F_c|^2)^2/\sum wF_o^4\}^{1/2}$, where $w=1/\sigma^2(F_o^2)]$ of 0·063 and a goodness-of-fit $\{=[\sum w(|F_o|^2-|F_c|^2)^2/(M-S)]^{1/2}$ for $M=4684$ observations and $S=135$ parameters$\}$ of 1·62 for all reflections. The largest shift in the final least-squares calculation was $0{\cdot}26\sigma$ for a hydrogen isotropic temperature factor. Scattering factor were those in *International Tables for X-ray Crystallography* (1962) except for hydrogen (Stewart, Davidson & Simpson, 1965).

The final positional and thermal parameters appear in Table 2. The final value of the secondary extinction parameter, g (Larson, 1967, equation 3), was $1{\cdot}6\ (3)\times 10^{-6}$.

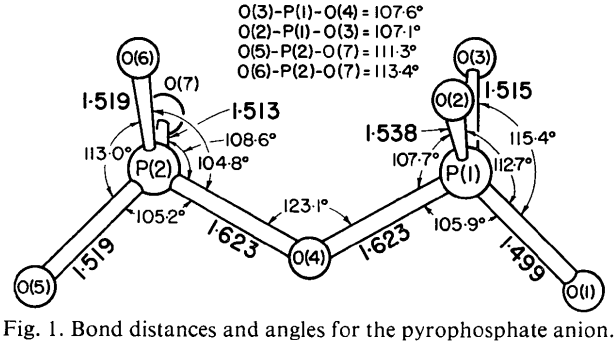

Fig. 1. Bond distances and angles for the pyrophosphate anion.

Discussion

Bond distances and angles for the pyrophosphate anion are shown in Fig. 1; standard deviations as evaluated from the coordinate uncertainties in Table 2 are approximately 0·001 Å and 0·06°. The P–O_T (terminal) distances range from 1·499 to 1·538 Å, the O_B(bridge)–P–O_T angles from 104·8° to 108·6°, and the O_T–P–O_T angles from 107·1° to 115·4°. These relatively large variations are typical as evidenced in Table 3, where we have collected the dimensions of the pyrophosphate ion as found in various crystal structures. In the present instance, at least, the variations in the P–O_T distances appear to be correlated with the number and strength of the Ca···O and O–H···O interactions as shown in Table 4. The longest P–O_T distance involves O(2), which is the only oxygen atom to have three Ca^{2+} ions as near neighbors. The shortest P–O_T distance involves the only atom to have a single Ca^{2+} ion and a single water molecule as neighbors. The re-

Table 2. *Coordinates and anisotropic temperature factors*

Coordinates and anisotropic parameters $\times 10^4$; standard deviations are given in parentheses. The anisotropic temperature factor has the form $\exp[\beta_{11}h^2+\beta_{22}k^2+\beta_{33}l^2+\beta_{12}hk+\beta_{13}hl+\beta_{23}kl]$.

	x	y	z	β_{11}	β_{22}	β_{33}	β_{12}	β_{13}	β_{23}
Ca(1)	2485 (1)	5056 (1)	3100 (1)	45 (1)	33 (1)	42 (1)	14 (1)	−30 (1)	13 (1)
Ca(2)	8645 (1)	7566 (1)	2603 (1)	50 (1)	29 (1)	48 (1)	−5 (1)	−37 (1)	28 (1)
P(1)	9893 (1)	1873 (1)	2601 (1)	38 (1)	23 (1)	41 (1)	0 (1)	−36 (1)	16 (1)
P(2)	7124 (1)	3559 (1)	1667 (1)	34 (1)	28 (1)	43 (1)	1 (1)	−35 (1)	16 (1)
O(1)	10168 (2)	85 (1)	2516 (2)	65 (2)	24 (1)	91 (2)	−1 (2)	−63 (3)	34 (2)
O(2)	9849 (2)	2984 (1)	4790 (2)	68 (2)	40 (1)	50 (2)	24 (2)	−62 (3)	−7 (2)
O(3)	11346 (1)	2632 (1)	918 (2)	49 (2)	48 (1)	57 (2)	−17 (2)	−43 (3)	39 (3)
O(4)	7825 (1)	1956 (1)	2232 (1)	40 (2)	31 (1)	74 (2)	−7 (2)	−48 (3)	39 (2)
O(5)	5039 (1)	3204 (1)	1791 (2)	36 (2)	53 (1)	86 (2)	10 (2)	−51 (3)	20 (3)
O(6)	7426 (2)	5007 (1)	3393 (2)	77 (2)	31 (1)	60 (2)	−5 (2)	−70 (3)	14 (2)
O(7)	8288 (1)	3713 (1)	−566 (2)	55 (2)	56 (1)	54 (2)	8 (2)	−27 (3)	55 (3)
O(8)	5031 (2)	7433 (2)	2536 (2)	83 (2)	60 (2)	85 (2)	23 (3)	−62 (4)	28 (3)
O(9)	3334 (2)	652 (2)	3995 (2)	68 (2)	72 (2)	100 (3)	0 (3)	−60 (4)	43 (3)

	x	y	z	B		x	y	z	B
H(1)	5223 (41)	7440 (37)	1141 (51)	4·84 (73)	H(3)	2526 (35)	315 (31)	3501 (39)	2·51 (50)
H(2)	4719 (36)	8352 (35)	3099 (44)	3·04 (56)	H(4)	4121 (44)	1234 (39)	3245 (50)	4·84 (74)

Table 3. *Comparison of dimensions in various pyrophosphate anions*

Uncertainties in distances and angles are calculated from coordinate uncertainties and are denoted by brackets. The average differences from the mean P–O_B distances are quoted in parentheses.

	P–O_T (Å)	$\overline{\text{P–O}_B}$ (Å)	P–O_B–P (°)	O_B–P–O_T (°)	O_T–P–O_T (°)	$\overline{O_T\text{–P}\cdots\text{P–}O_T}$(°)	Reference
$Ca_2P_2O_7.2H_2O$	1·499–1·538 [1]	1·623 [1] (0)	123·0° [6]	104·8–108·6 [1]	107·1–115·4 [1]	23·4	1
β-$Ca_2P_2O_7$ 1	1·480–1·530 [10]	1·627 [10] (10)	130·5° [5]	101·9–109·6 [5]	109·2–116·9 [5]	9·1	2
2	1·498–1·562 [10]	1·603 [10] (13)	137·8° [5]	101·6–108·3 [5]	108·9–115·0 [5]	16·6	
α-$Ca_2P_2O_7$†	1·493–1·538 [9]	1·598 [9] (19)	130·0° [4]	105·3–110·5 [5]	108·8–114·8 [5]	19·5	3
α-$Cu_2P_2O_7$*	1·508–1·547 [6]	1·576 [3] (–)	156·6° [1·1]	104·0–112·1 [5]	110·4–113·7 [4]	60§	4
β-$Cu_2P_2O_7$†*	1·503–1·518 [7]	1·542 [2] (–)	180·0° [–]	105·4–108·7 [2]	111·1–111·1 [3]	60§	5
α-$Mg_2P_2O_7$	1·472–1·539 [5]	1·591 [4] (22)	144·0° [5]	102·2–110·3 [3]	111·2–115·0 [3]	58·7	6
β-$Mg_2P_2O_7$†*	1·534–1·542 [6]	1·557 [2] (–)	180·0° [–]	106·8–107·4 [2]	111·5–112·6 [2]	60§	7
α-$Zn_2P_2O_7$ 1*	1·512–1·541 [8]	1·603 [6] (–)	138·7° [7]	103·2–112·2 [4]	109·7–113·3 [5]	60§	8
2	1·489–1·531 [8]	1·583 [8] (17)	148·4° [5]	103·2–111·1 [5]	111·2–114·4 [5]	57·8	
β-$Zn_2P_2O_7$†	1·554–1·556 [15]	1·569 [5] (–)	180·0° [–]	102·2–109·9 [5]	110·8–112·7 [6]	60§	7
$Cd_2P_2O_7$	1·449–1·558 [15]	1·625 [13] (20)	132·3° [7]	102·9–110·1 [7]	106·8–116·8 [9]	9·2	9
$Na_4P_2O_7.10H_2O$*	1·510–1·526 [5]	1·612 [5] (–)	130·2° [5]	102·0–108·9 [2]	111·1–114·4 [3]	60§	10
$K_4P_2O_7.3H_2O$	1·492–1·517 [6]	1·636 [5] (13)	130·3° [3]	102·1–108·3 [3]	111·5–114·3 [4]	46·9	11

References: (1) This work. (2) Webb (1966). (3) Calvo (1968). (4) Robertson & Calvo (1967). (5) Robertson & Calvo (1968). (6) Calvo (1967). (7) Calvo (1965*a*). (8) Robertson & Calvo (1970). (9) Calvo & Au (1969). (10) McDonald & Cruickshank (1967). (11) Dumas & Galigné (1974).

* Pyrophosphate anion contains a symmetry element.
† High temperature phase structure.
§ Pyrophosphate anion ideally staggered, thortveitite-type structure.

maining four O_T atoms show approximately equal P–O_T distances, and all have either two Ca^{2+} ions or one Ca^{2+} ion and two water molecules as neighbors. The six O_T atoms all have relatively small and comparable temperature factors, and there is no indication that the differences in P–O distances are due to librational effects. As would be expected, increasing the number of calcium and water molecule contacts with the terminal oxygen atoms leads to weaker and hence longer P–O_T bonds.

Table 4. *Terminal oxygen atom environment and its effect on the* P–O_T *distance in* $Ca_2P_2O_7.2H_2O$

Variances in calcium and water contacts are 0·001 and 0·002 Å respectively.

Oxygen No.	P–O_T	Ca···O_T		Ow···O_T	
1	1·499	2·285		2·758	
7	1·513	2·386	2·450		
3	1·515	2·320	2·447		
5	1·519	2·362		2·838	2·839
6	1·519	2·339	2·379		
2	1·538	2·366	2·463	2·642	

The remarkable flexibility of the pyrophosphate anion is evidenced in the variation in the P–O_B–P angle (Table 3), which ranges from 123° in the present structure to a formal value of 180° in compounds having the thortveitite-type structure. (While the space-group symmetry of the thortveitite structure requires the P–O_B–P bond to be linear, the temperature factors of the O_B atom are somewhat larger than for the P atoms, and have been interpreted by some (Calvo, 1965*a*,*b*) as representing disorder of two or more slightly non-linear structures.) The value of this P–O_B–P bond angle correlates well with the P–O_B distance (see Fig. 2); the longest P–O_B distances, about 1·62–1·63 Å, accompany the smallest P–O_B–P angles and the shortest distances, about 1·54–1·56 Å, accompany the largest angles.

This relationship is not entirely unexpected; an increased P–O_B–P angle would allow for enhanced $d\pi$–$p\pi$ overlap in the P–O_B bonds (Cruickshank, 1961), resulting in a shorter P–O_B distance. The wide range in bridging angles probably implies little change in

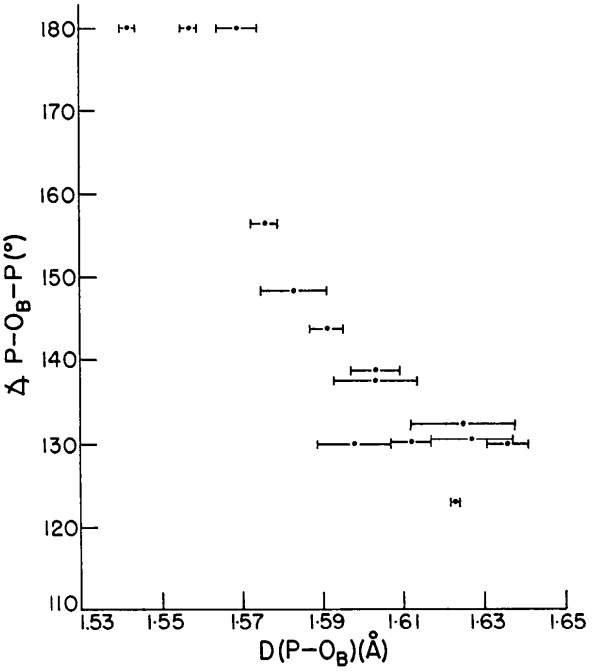

Fig. 2. This graph illustrates the strong relationship between the phosphorus–bridging oxygen bond length and the bridging angle. Indicated uncertainties were taken directly from $\overline{\text{P–O}_B}$ uncertainties in Table 3.

energy as the geometry of the ion changes from a severely bent configuration with relatively long P–O_B distances to a linear configuration with shorter P–O_B distances.

The conformational angles about the P–O_B bonds also cover a wide range, the terminal PO_3 groups being eclipsed in some cases and staggered in others. In the present structure these groups are approximately eclipsed (see Fig. 3), the average torsion angle O_T–P···P–O_T being 23·4°; they are also eclipsed in the anhydrous forms of $Ca_2P_2O_7$, the corresponding averages being 19·5° for α-$Ca_2P_2O_7$ and 9·1° and 16·6° for the two independent molecules in β-$Ca_2P_2O_7$.

The structure of $Ca_2P_2O_7.2H_2O$ is shown in Fig. 4, which emphasizes the coordination about the Ca^{2+} ions, and in Fig. 5, which emphasizes the hydrogen bonding. Details of the calcium coordination are given in Table 5, and of the hydrogen bonds in Table 6. Both Ca^{2+} ions are seven-coordinate, the polyhedron about Ca(1) being a capped octahedron and that about Ca(2) being a distorted pentagonal bipyramid. In contrast,

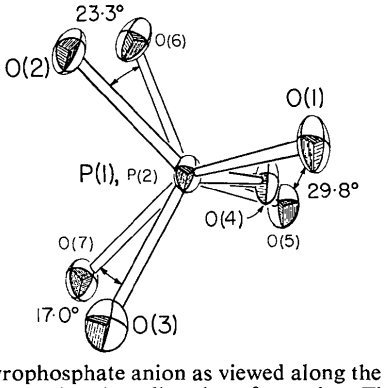

Fig. 3. The pyrophosphate anion as viewed along the P(1), P(2) direction illustrating the eclipsed conformation. The average of the depicted torsion-angle magnitudes is 23·4°.

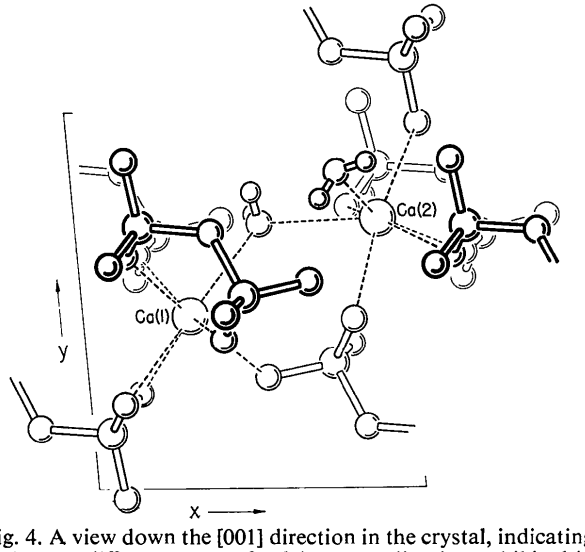

Fig. 4. A view down the [001] direction in the crystal, indicating the two different types of calcium coordination exhibited in $Ca_2P_2O_7.2H_2O$.

Table 5. *Interatomic distances* (Å) *in the calcium–oxygen coordination polyhedron*

The values in brackets are unit-cell translations and equivalent position numbers (where equivalent position 1 is x,y,z, and 2 is $\bar{x},\bar{y},\bar{z}$). Variances are of the order of 0·001 Å.

Ca(1)		Ca(2)	
O(2)[$\bar{1}$00,1]	2·642	O(1)[010,1]	2·285
O(2)[111,2]	2·366	O(2)[211,2]	2·463
O(3)[$\bar{1}$00,1]	2·447	O(3)[210,2]	2·320
O(5)[000,1]	2·362	O(6)[000,1]	2·339
O(6)[111,2]	2·379	O(7)[210,2]	2·450
O(7)[110,2]	2·386	O(8)[000,1]	2·668
O(8)[000,1]	2·608	O(9)[111,2]	2·526

Table 6. *Details of the water molecules and their hydrogen bonds*, O–H···*A*

Hydrogen bonds

O–H···*A*	O···*A*	H···*A*	∠O–H···*A*
O(8)–H(1)···O(5)	2·838 (2) Å	1·974 (30) Å	159 (3)°
O(8)–H(2)···O(9)	2·885 (2)	2·121 (26)	162 (3)
O(9)–H(3)···O(5)	2·839 (2)	2·055 (27)	156 (3)
O(9)–H(4)···O(1)	2·758 (2)	2·006 (30)	164 (2)

Water molecules

	O–H	∠H–O–H
O(8)–H(1)	0·90 (3) Å	102 (2)°
O(8)–H(2)	0·79 (3)	
O(9)–H(3)	0·84 (3)	111 (3)
O(9)–H(4)	0·77 (3)	

the two Ca^{2+} ions in the high-temperature form of anhydrous $Ca_2P_2O_7$ (Calvo, 1967) are eight-coordinate, while the four independent Ca^{2+} ions in the low-temperature form of $Ca_2P_2O_7$ (Webb, 1966) have coordination numbers of 7, 7, 8, and 9.

The structures of the three known forms of $Ca_2P_2O_7$ provide eloquent evidence as to the exceptional versatility of the $P_2O_7^{4-}$ ion as a ligand. Although in many instances it is monodentate, it can also serve as a bidentate ligand in one of three different ways: (1) by using two terminal oxygen atoms on the same phosphorus atom, (2) by using a terminal oxygen atom on each of the two phosphorus atoms, (3) or by using one terminal oxygen atom together with the bridging oxygen atom. This versatility of function, together with the extreme flexibility of the P–O_B–P angle, P–O_T distance, and torsional conformation, allows the $P_2O_7^{4-}$ ion to adapt to a wide range of structures.

With the crystal structure in hand, what can be said about the mode of action of the calcium pyrophosphate dihydrate crystals in the gouty type inflammation? Some physiological imbalance creates an excess of pyrophosphate ions due either to decreased activity of the enzyme pyrophosphatase or perhaps due to localized excess production of the ion. The available pyrophosphate ions then complex with calcium ions, which are always in high concentration in the human body, forming very insoluble crystallites. If all proceeded as nature prescribed, the dihydrate crystals

would be engulfed and digested by the lysosome as though they were foreign bodies. This unfortunately is not the situation. The crystals are engulfed, but before digestion can take place the lysosomal membrane ruptures. This rupture allows the lysosomal enzymes to escape and begin uncontained random digestion. This membrane rupture only occurs after the crystal is within the lysosome, and in particular, when the crystal and membrane are proximal.

The most probable mechanism for the membrane rupture (Weissmann & Rita, 1972) involves hydrogen bonding between the inflammatory crystals and the polar phosphate heads of the phospholipid molecules in the lysosomal membrane. In this scheme the crystals would contain the hydrogen-bond donors, and the oxygen atoms of the phosphate ends of the phospholipid molecules would be the acceptors. Model building and low-angle X-ray scattering experiments on membranes have indicated a hexagonal array of phospholipid molecules with a phosphate repeat distance between phosphate groups of 4·5 to 4·8 Å (Träuble & Sackmann, 1972). Electron microscope studies (Mandel, 1975) on *in vivo* pseudogout samples have indicated that the two largest faces in the crystal, the (100) and the (01$\bar{1}$), are those which most frequently interact with the membrane. As seen in Fig. 5, the (100) face is rich in both calcium ions and water molecules which may be used in the membrane interaction. Inspection of the (100) and the (01$\bar{1}$) projections has unfortunately not answered the question as to whether the calcium ions and water molecules interact separately or cooperatively with the membrane. This ambiguity will hopefully be resolved after the remainder of our studies on all gouty inflammatory crystals have been completed.

I would like to thank Miss Lillian Casler for help in the preparation of the illustrations and Dr Sten Samson for his expert assistance during data collection. I would especially like to thank Dr Gretchen Mandel and Dr R. E. Marsh for numerous discussions during the structure solution and the preparation of this manuscript. I would like to thank the Arthritis and Metabolic Disease Institute of the National Institutes of Health for a postdoctoral fellowship.

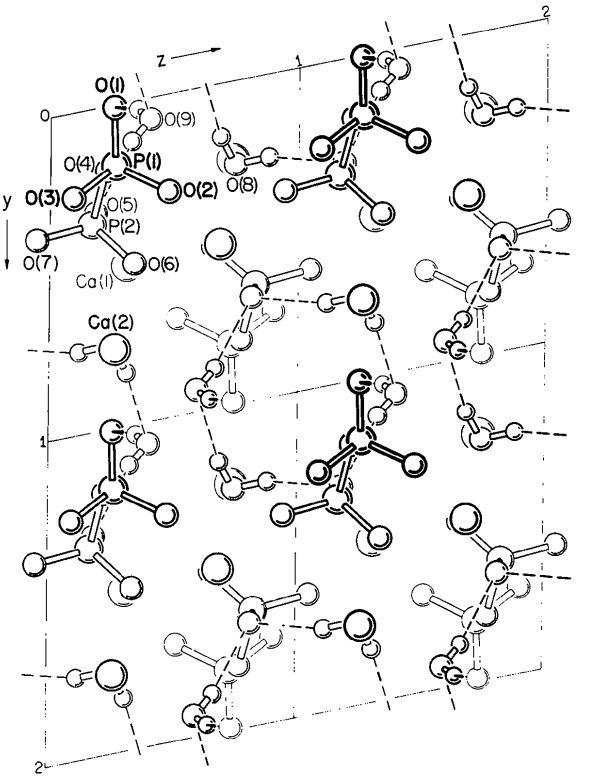

Fig. 5. A view down the [100] direction illustrating the hydrogen bonding between the water molecules and the pyrophosphate anions.

References

BROWN, E. H., LEHR, J. R., SMITH, J. P. & FRAZIER, A. W. (1963). *Agric. Food Chem.* **11**, 214–222.

CALVO, C. (1965*a*). *Canad. J. Chem.* **43**, 1139–1146.

CALVO, C. (1965*b*). *Canad. J. Chem.* **43**, 1147–1153.

CALVO, C. (1967). *Acta Cryst.* **23**, 289–295.

CALVO, C. (1968). *Inorg. Chem.* **7**, 1345–1351.

CALVO, C. & AU, P. K. L. (1969). *Canad. J. Chem.* **47**, 3409–3416.

CRUICKSHANK, D. W. J. (1961). *J. Chem. Soc.* pp. 5486–5504.

DUMAS, Y. & GALIGNÉ, J. L. (1974). *Acta Cryst.* B**30**, 390–395.

International Tables for X-ray Crystallography (1962). Vol. III, pp. 201–207. Birmingham: Kynoch Press.

LARSON, A. C. (1967). *Acta Cryst.* **23**, 664–665.

MCDONALD, W. S. & CRUICKSHANK, D. W. T. (1967). *Acta Cryst.* **22**, 43–48.

MANDEL, N. S. (1975). To be published.

ROBERTSON, B. E. & CALVO, C. (1967). *Acta Cryst.* **22**, 665–672.

ROBERTSON, B. E. & CALVO, C. (1968). *Canad. J. Chem.* **46**, 605–612.

ROBERTSON, B. E. & CALVO, C. (1970). *J. Solid State Chem.* **1**, 120–133.

STEWART, R. F., DAVIDSON, E. R. & SIMPSON, W. T. (1965). *J. Chem. Phys.* **42**, 3175–3186.

TRÄUBLE, H. & SACKMANN, E. (1972). *J. Amer. Chem. Soc.* **94**, 4499–4510.

WEBB, N. C. (1966). *Acta Cryst.* **21**, 942–948.

WEISSMANN, G. & RITA, C. A. (1972). *Nature, New Biol.* **240**, 167–172.